International Journal of Energy Production and Management
https://www.acadlore.com/journals/IJEPM

Assessment of a Photovoltaic-Driven Pumped Hydro Storage with Multi-Pump Operation and Cascading Turbines

Syafii*, Fauzan Wafi, Novizon, Rizki Wahyu Pratama

Departement of Electrical Engineering, Engineering Faculty, Universitas Andalas, 25175 Padang, Indonesia

* Correspondence: Syafii (syafii@eng.unand.ac.id)

Received: 09-29-2025 **Revised:** 11-20-2025 **Accepted:** 12-16-2025

Citation: Syafii, F. Wafi, Novizon, R. W. Pratama, "Assessment of a photovoltaic-driven pumped hydro storage with multi-pump operation and cascading turbines," *Int. J. Energy Prod. Manag.*, vol. 10, no. 4, pp. 576–589, 2025. https://doi.org/10.56578/ijepm100402.

Abstract: This study presents the design and experimental evaluation of a laboratory-scale Pumped Hydro Storage (PHS) system driven by photovoltaic (PV) power, featuring adaptive multi-pump operation and a cascading turbine–generator configuration. The system integrates real-time monitoring and control architecture based on ESP32 and NRF24L01 modules with a Raspberry Pi web interface, allowing automatic operation according to PV power availability and reservoir conditions. The adaptive multi-pump mechanism enables stepwise pump activation as solar energy increases, effectively balancing water transfer and electrical consumption. Experimental results demonstrate that increasing the number of operating pumps significantly improves flow rate and upper reservoir elevation, confirming the effectiveness of the adaptive strategy under variable PV conditions. Furthermore, comparative testing of cascading turbine–generator configurations indicates that the parallel configuration achieves higher conversion efficiency and energy yield than the series configuration. These findings validate that multi-pump adaptive control combined with an optimized turbine configuration enhances the flexibility and overall efficiency of small-scale PHS systems. The proposed architecture offers a practical framework for integrating solar energy and hydro storage technologies to support reliable and sustainable off-grid power applications.

Keywords: PHS; PV power; Pumped hydro; Turbine–generator configuration; Energy storage

1 Introduction

The transition to a low-carbon, environmentally friendly electricity system has become a global urgency in addressing climate change and the energy crisis. Fossil fuels, particularly coal, still contribute around 25% of global greenhouse gas emissions [1]. Indonesia has set an emission reduction target through the Enhanced Nationally Determined Contribution (NDC) document of 31.89% unconditionally and 43.20% conditionally by 2030 [2], and a long-term vision of carbon neutrality by 2060 or sooner [3]. Solar energy is seen as one of the main solutions because of its huge potential, which is around 208 GW with an average daily radiation of 4.8–5.1 $\mathrm{kWh/m^2}$ [4, 5]. However, the intermittent nature of PV system due to fluctuations in solar irradiation creates limitations on their use, especially in small-scale or off-grid systems [6]. Therefore, energy storage technology is needed that is capable of absorbing surplus power and releasing it again when a deficit occurs [7, 8].

One promising technology is Pumped Hydro Storage (PHS), an energy storage system that converts excess electrical power into hydro potential energy by pumping water from a lower reservoir to an upper reservoir, then generating electricity again through a turbine when the water flows down [9, 10]. Unlike conventional hydropower plants or microhydro power plants which are open-loop and depend on natural water sources, PHS can operate in a closed-loop scheme, making it more flexible to be applied to standalone systems [11]. However, the conventional PHS configuration with one pump and one turbine still has limitations, namely the pump has a fixed capacity and is not adaptive to variations in solar power, and the use of one turbine limits the energy conversion path. Therefore, a multi-pump operation strategy is needed that can be activated selectively according to power availability [12], as well as a cascading turbine-generator configuration (series or parallel) to optimize energy conversion [13].

Several previous studies have highlighted these aspects, but their scope remains limited. According to study [14], under low test flow conditions, a series configuration appears relatively superior; however, at higher flow rates, a

parallel configuration tends to provide better overall performance because each turbine operates at near-full head. However, these studies have not integrated adaptive control in the context of a PHS. The research presented in study [15–17] emphasize the importance of PHS in off-grid hybrid systems based on solar power plants, wind, and biogas, but their study was based on simulations using HOMER Pro without real-time control or monitoring. The developement of an adaptive multi-pump concept through MATLAB/Simulink simulations and demonstrated potential efficiency improvements, but this has not yet been implemented in hardware [12]. At the practical application level, study [18] designed a PLC and Arduino-based solar pump automation system focusing on pump protection through monitoring of flow and water level. Although successful in automatically regulating pump operation, this approach is still limited to a single pump unit and does not support the integration of wireless communication or remote monitoring.

Addressing these limitations, this study developed a laboratory-scale closed-loop PHS system with two key innovations: (i) adaptive multi-pump operation that is activated step by step according to solar power availability, and (ii) experimental evaluation of cascading turbine–generator configurations, both series and parallel, within a single prototype platform. The control system was built using an ESP32 microcontroller at each node, an NRF24L01 wireless module for communication, and a Flask-based Raspberry Pi interface for real-time monitoring and control. With this approach, operational decisions—from pump activation to turbine configuration selection—are based on field data in the form of PV output power, discharge, water level, and reservoir volume. This study contributes by providing experimental evidence of the advantages of parallel configurations over series, while also demonstrating an efficient, responsive, and applicable adaptive PHS architecture in supporting solar energy utilization in small-scale off-grid systems.

2 Literature Review

2.1 PV System

PV system are electrical energy generation systems derived from solar radiation. This light energy is converted into electrical energy through solar panels composed of numerous photovoltaic cells. Based on their operating method, PV system are divided into two types: on-grid, which are directly connected to the electricity grid; and off-grid, which operate independently [19, 20]. Off-grid systems generally use a DC-coupling configuration, where solar panels channel energy to the battery through a charge controller, which is then converted into AC current by an inverter to supply the load [21].

Solar cells consist of N-type (negative) and P-type (positive) semiconductor layers. When photons of sunlight hit the cell surface, the photon energy releases electrons from the semiconductor material. The released electrons move from the N-type to the P-type layer, producing direct current (DC). This mechanism is known as the photovoltaic effect and is the basis of energy conversion in solar panels [22, 23].

Each solar cell produces a relatively small voltage, so to increase the voltage, a series arrangement is used. In this circuit, the positive terminal of one cell is connected to the negative terminal of the next cell, so that the total voltage is the sum of the voltages of each cell, while the current remains constant. This series arrangement creates a solar module with a higher voltage, according to the system's needs [24]. Conversely, in a parallel circuit, the positive terminals of each cell are connected together, as are their negative terminals. This configuration makes the total current increase according to the number of cells, while the voltage remains the same as for one cell [25]. The parallel configuration is suitable for systems that require a large current but still maintain a low to medium voltage.

2.2 Solar Panel Efficiency

Solar panel efficiency is defined as the ratio between the maximum electrical power output of a photovoltaic module and the solar radiation power received by its surface [26]. In general, it can be written as:

$$\eta = \frac{P_{\text{out}}}{P_{\text{in}}} \times 100\% \tag{1}$$

$$P_{\text{out}} = V_{\text{mpp}} \times I_{\text{mpp}} \tag{2}$$

$$P_{in} = G \times A \tag{3}$$

PV module performance is generally evaluated through the I-V curve which produces important parameters, namely short circuit current (Isc), open voltage (Voc), and maximum power point (V_{mpp}, I_{mpp}) [27]. To assess the quality of the I-V curve, the fill factor is used:

$$FF = \frac{V_{mpp} \times I_{mpp}}{V_{oc} \times I_{sc}} \tag{4}$$

So the module efficiency can also be written as:

$$\eta = \frac{V_{oc} \times I_{sc} \times FF}{G \times A} \tag{5}$$

In manufacturing tests, the efficiency of PV modules is usually determined under Standard Test Conditions (STC), namely 1000 $\mathrm{W/m^2}$ irradiance, 25 °C cell temperature, and AM 1.5 light spectrum [28]. This efficiency value is known as the nominal efficiency. However, under field operational conditions, the actual efficiency is almost always lower because the module is exposed to temperature variations, spectrum changes, partial shade, and deviations in tilt angle [29]. The direct relationship between solar irradiance and panel output power can be expressed as:

$$P_{\text{out}} = \eta \times G \times A \tag{6}$$

Solar modules have high efficiency under standard conditions, variations in environmental factors cause their actual performance to fluctuate. In this study, the panel output power, P_{out}, was used as a reference to determine the pump activation threshold. This ensures the PHS system can adaptively adjust the number of pumps operating based on the available PV power.

2.3 Pumped Hydro Storage (PHS)

Pumped Hydro Storage (PHS) is an energy storage technology that utilizes the difference in elevation between two water reservoirs (upper and lower) to store and generate electricity [30]. When there is a power surplus, typically from a solar power plant during the day, the electrical energy is used to pump water from the lower reservoir to the upper reservoir, storing it as gravitational potential energy. This energy is then released when the power supply from the solar power plant decreases or load demand increases, by flowing water from the upper reservoir to the lower reservoir through a turbine connected to a generator [31–33].

The PHS system operates in two main modes. In charging mode, excess electricity is used to pump water to the upper reservoir, while in discharging mode, water from the upper reservoir flows down to rotate the turbine and generate electricity. With this mechanism, PHS acts as an energy storage device capable of balancing the intermittent availability of solar power [34]. A well-thought-out research design ensures that the data obtained from this experiment is valid and meets the research objectives.

2.4 Potential Energy in a PHS Reservoir

Water potential energy is the energy possessed by a mass of water due to its position at a certain height relative to the Earth's reference surface. The amount of this energy is influenced by the mass of the water (m), gravitational acceleration (g), and the height difference (H) between the upper reservoir and the turbine [31, 35]. This relationship is formulated as:

$$E = m \times g \times H \tag{7}$$

In the context of PHS, the mass of water can be written as the product of the water density (ρ) and the water volume (V):

$$m = \rho \times V \tag{8}$$

Therefore, the gravitational potential energy of the water in the reservoir is:

$$E = \rho \times V \times g \times H \tag{9}$$

This equation explains that the energy stored in the reservoir depends on the water volume, the height difference (head), and the gravitational constant. If water is discharged at a flow rate of $Q\ (m^3/s)$, then the volume of water flowing in time t is:

$$V = Q \times t \tag{10}$$

Therefore, the energy that can be released from the reservoir can be written as:

$$E = \rho \times (Q \times t) \times g \times H \tag{11}$$

This formula forms the basis for calculating energy capacity in a PHS system. The greater the volume of water displaced and the greater the height difference, the greater the potential energy that can be stored or converted into electrical energy through a turbine.

The reviewed literature provides the theoretical foundation and motivation for this study by identifying current limitations in solar-powered Pumped Hydro Storage (PHS) research. Most previous works have focused on simulations or single-pump systems without adaptive control or experimental validation, while the performance comparison of cascading turbine–generator configurations has rarely been examined under real operating conditions. These findings highlight the need for a practical PHS prototype capable of adaptive multi-pump operation and real-time performance evaluation. Therefore, this study develops a laboratory-scale PHS system to experimentally validate adaptive pumping control and series–parallel turbine configurations in optimizing solar energy utilization.

3 Methodology

3.1 PHS System Operational Flow (Charging and Discharging)

This research is a laboratory-scale experimental study that designs a closed-loop PHS prototype integrated with a Solar Power Plant (PLTS). The system is designed to operate multiple pumps adaptively according to solar power availability and to test cascaded turbine-generator configurations in both series and parallel. In the context of the PHS system testing, two main operational flows are implemented: charging mode and discharging mode, as shown in Figure 1.

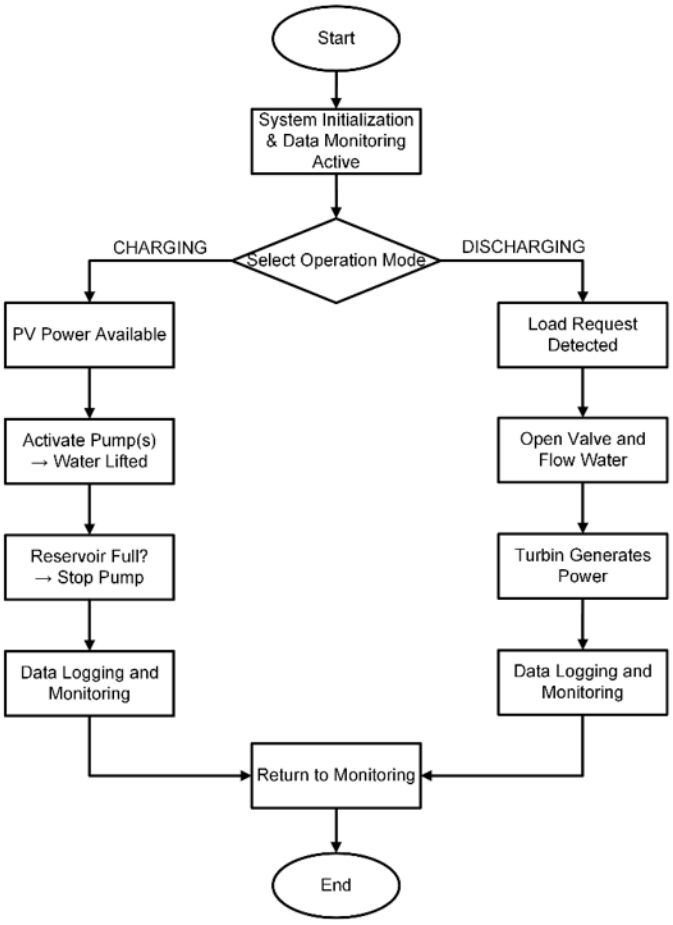

Figure 1. Operational flowchart of the pumped hydro storage system

Charging Mode: In this mode, the system monitors solar radiation intensity and the water levels in the upper and lower reservoirs. If solar radiation intensity is high, the upper reservoir is not yet full, and the lower reservoir has sufficient water, the charging process can begin. First, Valve 1 (lower reservoir output) is opened to ensure unobstructed water flow to the pump. The water pump (can be one or more pumps depending on the solar power available) is then activated to flow water to the upper reservoir. During pumping, flow sensors and ultrasonic sensors monitor the flow and water level in real time. The user or the system will stop the pump when the upper reservoir is full or has reached the desired level. The pump is turned off first, then Valve 1 is closed again to stop the flow from the lower reservoir, ending the charging mode.

Discharging Mode: The system monitors the electrical load demand (for example, during high loads or at night when PV is insufficient) and ensures that water is available in the upper reservoir. If energy demand exists and the upper reservoir has sufficient water volume, the discharging process can be initiated manually. First, Valve 2 (the upper reservoir output) is automatically opened via a control command, allowing pressurized water from the upper reservoir to flow into the microhydro turbine. This water flow rotates the turbine, which is connected to a generator, generating electricity based on the flow rate and height of the water drop. During discharge, sensors monitor the flow rate as well as the decrease in the water level in the upper reservoir and the increase in the lower reservoir. When the load is met or the water level in the upper reservoir approaches the minimum, Valve 2 is closed again, stopping the flow and electricity generation. Once the valve is closed, the energy discharge cycle is complete, and the system returns to monitoring mode (standby), ready to be recharged at the next opportunity.

After both modes have been executed as needed, one full PHS cycle has been completed (charge-discharge). The system can return to its initial monitoring mode, where sensors continue to actively monitor conditions, ready to operate again the next day or when solar energy is available again.

The developed PHS system architecture is shown in Figure 2. This system consists of distributed sensor-actuator nodes, a master unit as a connector, a local server, and a web interface. Each node is implemented using an ESP32 microcontroller equipped with sensors and actuators according to their functions.

1. Node 1 (ESP32) monitors water level and flow rate using ultrasonic and flow sensors, and controls valves via relays.
2. Node 2 (ESP32) is equipped with ultrasonic sensors, flow sensors, and a pyranometer to measure reservoir conditions and solar radiation intensity, with an additional relay for valve control.
3. Node 3 (ESP32) focuses on electrical monitoring and pump control, using two PZEM-017 sensors to measure voltage and current, and three motor drivers to control the pumps.

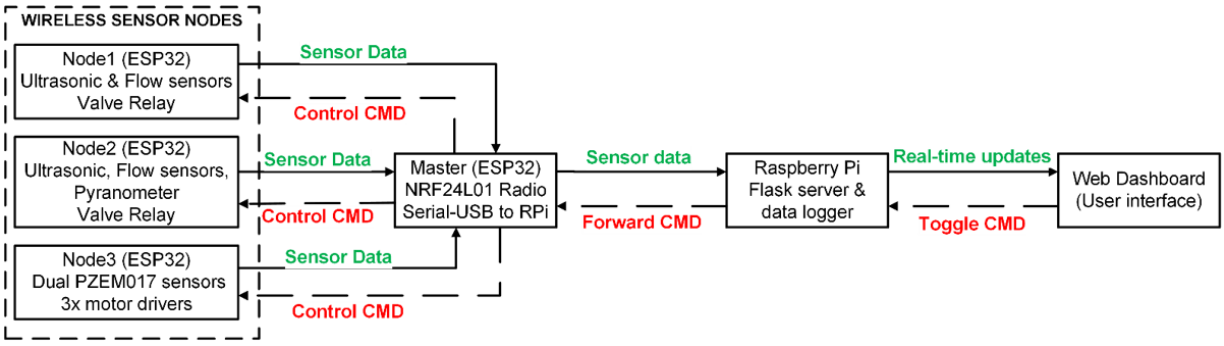

Figure 2. ESP32 multi-node based PHS system architecture

Data from all three nodes is sent wirelessly to the Master (ESP32) via the NRF24L01, then forwarded to the Raspberry Pi for real-time logging, monitoring, and control. A web dashboard serves as the primary user interface, displaying operational parameters and allowing pump and valve control commands. The system operates in a closed loop, enabling both monitoring and adaptive control.

In addition to real-time visualisation, the web dashboard acts as the main interface for system control: pump ON/OFF and valve open/close commands are issued on the Raspberry Pi, forwarded to the Master unit, and delivered to the target ESP node via NRF24L01. Conversely, sensor data from each node provide feedback to ensure that operation follows the actual system conditions, for example stopping pumping when the upper-reservoir level reaches the maximum setpoint or when PV power becomes insufficient. This establishes a closed-loop control structure that integrates measurement, wireless communication, and adaptive actuation. The combined PHS operational flow (charging–discharging) and IoT architecture are summarised in Figure 3, which presents the overall system control logic.

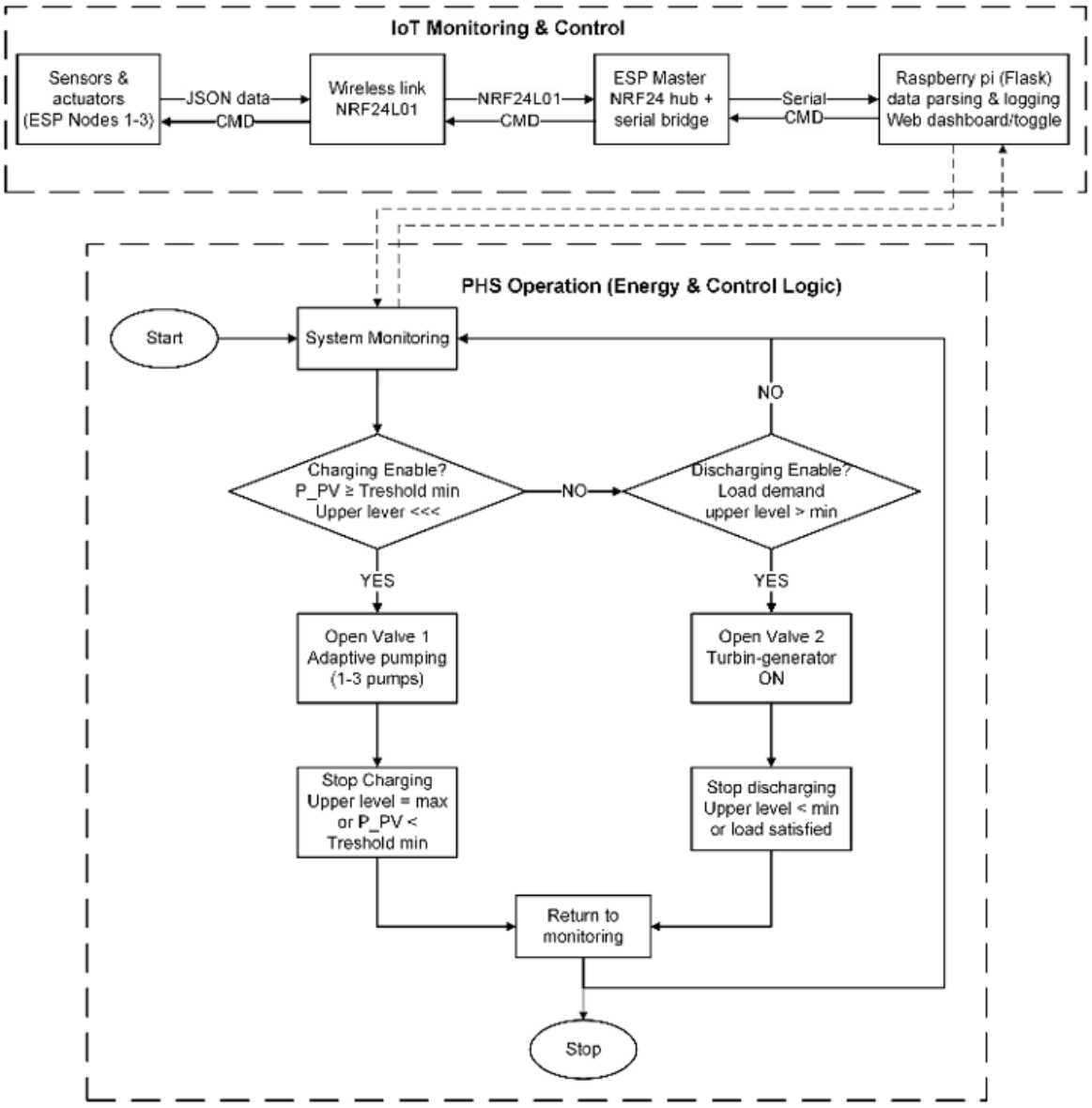

Figure 3. Overall control logic of the integrated PHS system

4 Result

4.1 Testing the Sensors

Sensor accuracy testing is carried out by comparing the sensor readings to reference measuring instruments, namely a FLUKE multimeter for voltage and current, a ruler for water level, and a solar power meter for solar irradiation.

Table 1. PZEM-017 sensor voltage test results

PZEM-017 (V)	Multimeter FLUKE (V)	Error (%)
7.7	7.6	1.316
8.5	8.4	1.190
10.8	10.7	0.935
	Mean	**1.147**

Based on Table 1 and Table 2, the PZEM-017 sensor shows an average measurement error of 1.15% (range 0.94–1.32%) for voltage and 0.46% (range 0.20–0.64%) for current, both of which are well below the ±5% tolerance, making them suitable for monitoring electrical parameters. The test results in Table 3 and Table 4 show that the

A02YYUW ultrasonic sensor in the lower reservoir produces an average error of 0.196% (range 0.118–0.235%) and in the upper reservoir 0.190% (range 0.114–0.343%), which is also well below the tolerance limit. The test results in Table 5 show that the pyranometer sensor has an average error of only 0.239% (range 0.23–0.26%) compared to the reference solar power meter. The validation tests were conducted under typical outdoor conditions, with ambient temperatures of approximately 27–33 °C and solar irradiance levels ranging from about 800 to 1000 W/m², as measured by the reference solar power meter. Therefore, all sensors used (PZEM-017, A02YYUW, and pyranometer) are proven to have high accuracy and are reliable for monitoring voltage, current, water level, and solar radiation intensity in the PHS system.

Table 2. PZEM-017 sensor current test results

PZEM-017 (V)	Multimeter FLUKE (V)	Error (%)
19.64	19.6	0.204
24.97	25.1	0.518
28.18	28	0.643
Mean		**0.455**

Table 3. Ultrasonic sensor accuracy test results A02YYUW in lower reservoir

A02YYUW (cm)	Ruler (cm)	Error (%)
84.8	85	0.235
84.9	85	0.118
85.2	85	0.235
Mean		**0.196**

Table 4. Ultrasonic sensor accuracy test results A02YYUW on upper reservoir

A02YYUW (cm)	Ruler (cm)	Error (%)
87.8	87.5	0.343
87.4	87.5	0.114
87.6	87.5	0.114
Mean		**0.190**

Table 5. Comparison of pyranometer readings with a reference solar power meter

Pyranometer $(\mathrm{W/m^2})$	Solar Power Meter $(\mathrm{W/m^2})$	Error (%)
971	973.5	0.257
868	870	0.230
863	865	0.231
Mean		**0.239**

4.2 Pump System Performance Analysis

Pump testing was conducted to evaluate how the number of operating pumps (1, 2, and 3 pumps) affects the performance of the PHS system, particularly the PV-side voltage, current, and power, as well as the resulting flow rate and the rise of the upper reservoir level. For each scenario, PV voltage–current and PV power profiles were plotted as functions of time and compared with the corresponding flow-rate and water-level responses to assess how effectively the available solar energy was converted into stored hydraulic energy by driving the pumps to transfer water from the lower to the upper reservoir. The ESP32–Raspberry Pi data-acquisition system was configured with a nominal sampling interval of 2 s, and the average and range values reported in this section were calculated only over the active pumping periods, with all idle intervals excluded from the analysis.

In Figure 4, the variation of PV load current and voltage during the 1-pump test is shown. The horizontal axis represents the actual operation time in hours and minutes (HH:MM), corresponding to the total pumping duration of 43.5 minutes (10:30:08–11:13:42). The left vertical axis indicates the pump current (A), while the right vertical axis represents the PV system voltage (V). When the pump is in the idle state, the current approaches 0 A and the PV voltage remains near the open-circuit level of 19–19.5 V. After activation, the pump draws a stable current of around

13.8 A (range 12.8–15.1 A), while the PV voltage decreases to approximately 15 V (range 14.4–15.8 V). This voltage drop reflects the shift of the PV operating point from a near open-circuit condition to a loaded region on the I–V curve as the pump draws power from the PV array.

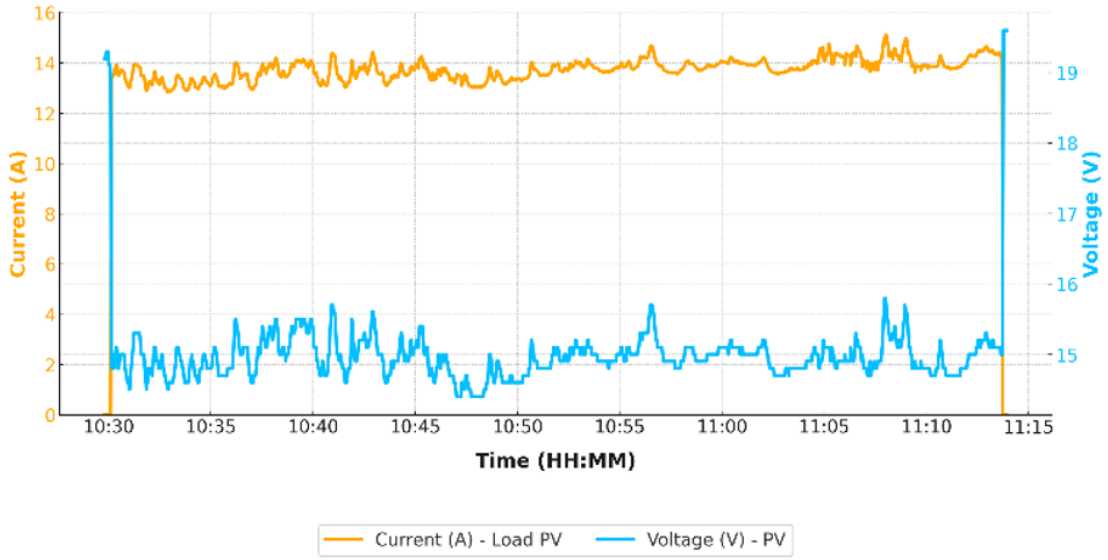

Figure 4. Result for single-pump operation

In Figure 5, the variation of PV power, flow rate, and upper reservoir water level during the single-pump test is presented. The horizontal axis represents the actual operation time in hours and minutes (HH:MM). The left vertical axis corresponds to PV power (W), while the right vertical axis corresponds to both flow rate (LPM) and upper reservoir water level (cm). PV power and flow rate increase when the pump is switched on, causing the upper-reservoir level to rise. The short spike at the beginning occurs because the pump and water flow are not yet fully stabilised. During the 1-pump operation, the PV power was around 205.7 W with a range of 186–238 W, indicating a fairly consistent solar-energy supply throughout the active phase. The average flow rate was approximately 0.66 LPM (range 0–1.61 LPM), whereas the upper reservoir level remained nearly constant at around 12.63 cm (range 2.0–12.7 cm) with a very slight upward trend. This observation indicates that, although sufficient PV power was available, the low discharge rate limited the increase of the upper reservoir water level during the single-pump test.

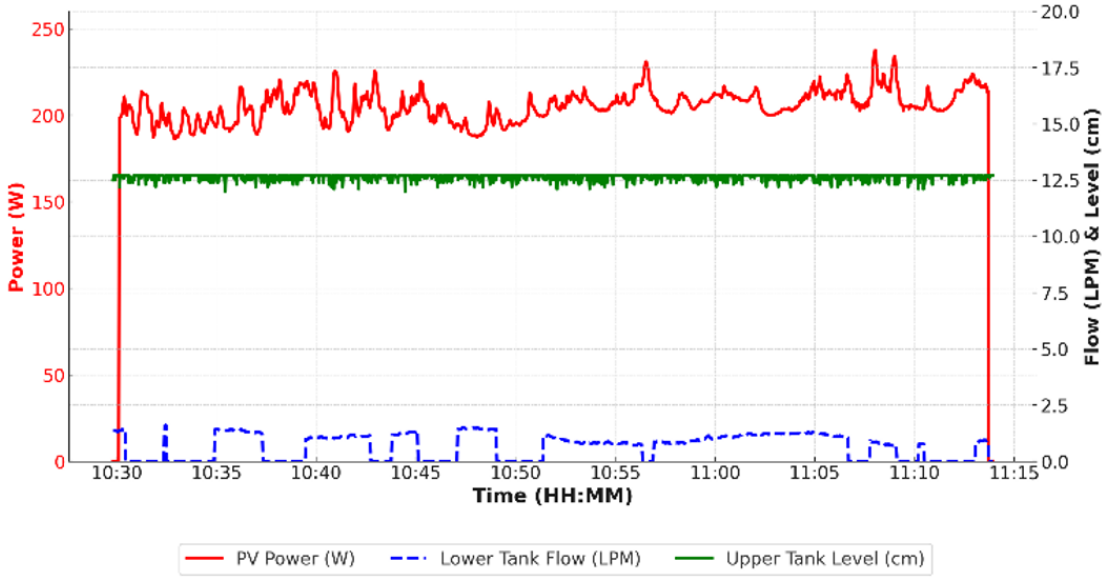

Figure 5. PV power, pump flow rate, and water level during single-pump operation

In Figure 6, the variation of PV voltage and load current during the 2-pump test is illustrated. The horizontal axis represents the actual operation time in hours and minutes (HH:MM). The left vertical axis corresponds to PV

voltage (V), while the right vertical axis corresponds to load current (A). When both pumps were inactive, the current approached 0 A and the PV voltage remained within the open-circuit range of 19–19.5 V. After the pumps were activated at 11:16:13 and operated until 11:49:59 (approximately 33 minutes and 46 seconds), the PV voltage dropped to the range of 11.50–14.30 V with an average of 12.42 V, while the load current increased to 16.63–22.24 A with an average of 19.45 A. This consistent decrease in PV voltage, together with the higher current, indicates that the operating point of the PV array shifted further along the I–V curve under the increased electrical load imposed by the two pumps operating simultaneously.

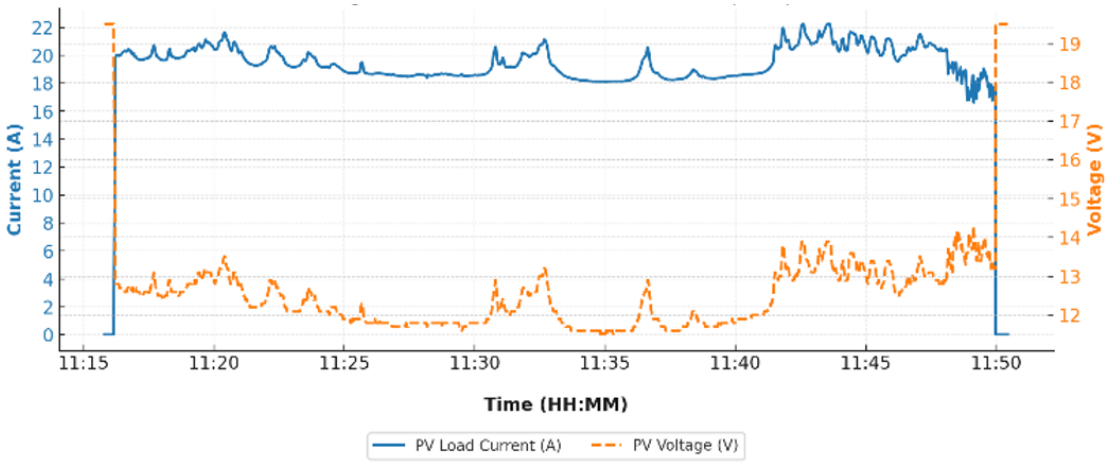

Figure 6. PV voltage and load current versus time for two-pump adaptive operation

In Figure 7, the variation of PV power, flow rate, and upper reservoir water level during the 2-pump test is shown. The horizontal axis represents the actual operation time in hours and minutes (HH:MM). The left vertical axis corresponds to PV power (W), while the right vertical axis corresponds to both flow rate (LPM) and upper reservoir level (cm). Operating two pumps produces higher PV power and flow rate, so the upper reservoir is filled more quickly. The brief spike at the start appears because the system has just been switched on and the flow is still stabilizing. Before the pumps were activated, the current remained nearly zero (0.00–0.02 A), while the PV voltage stayed within the open-circuit range of 18.80–19.20 V. Once all three pumps were switched on at 10:22:56 and operated until 10:45:37 (a total duration of approximately 22 minutes and 41 seconds), the current increased substantially to 15.18–29.10 A with an average of 24.31 A, while the voltage decreased to 7.70–15.40 V with an average of 9.77 V. This pronounced voltage drop, together with the large increase in current, confirms the expected behaviour of the PV system under maximum loading, where the operating point is driven further along the I–V curve as three pumps draw power simultaneously.

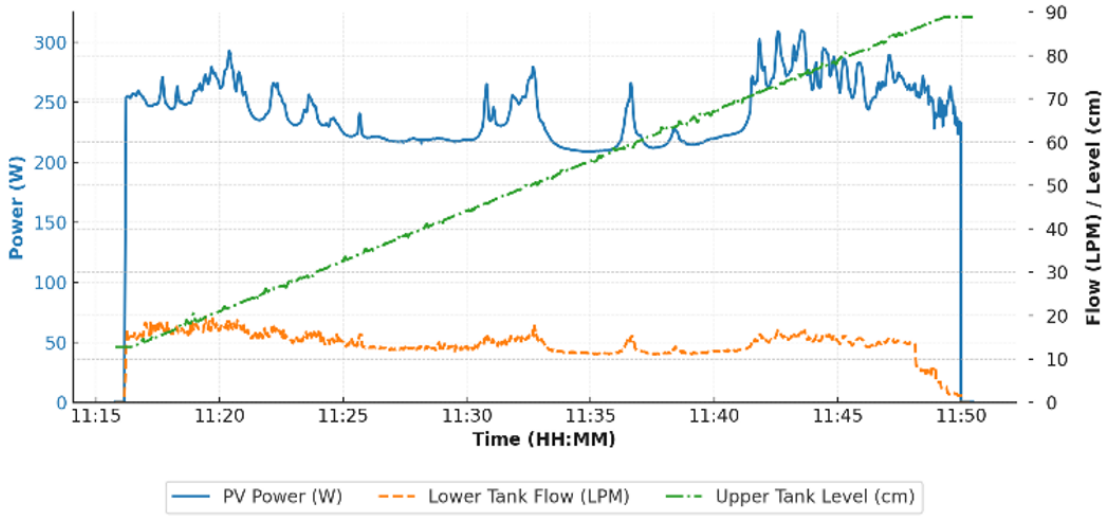

Figure 7. PV power, flow rate, and water level during two-pump operation

In Figure 8, the variation of PV load current and voltage during the 3-pump test is presented. The horizontal axis

represents the actual operation time in hours and minutes (HH:MM). The left vertical axis corresponds to PV load current (A), while the right vertical axis corresponds to PV system voltage (V). Before the pumps were activated, the current remained nearly zero (0.00–0.02 A), while the PV voltage stayed within the open-circuit range of 18.80–19.20 V. Once all three pumps were switched on at 10:22:56 and operated until 10:45:37 (a total duration of approximately 22 minutes and 41 seconds), the current increased substantially to 15.18–29.10 A with an average of 24.31 A, while the voltage decreased to 7.70–15.40 V with an average of 9.77 V. This pronounced voltage drop, together with the large increase in current, confirms the expected behaviour of the PV system under maximum loading, where the operating point is driven further along the I–V curve as three pumps draw power simultaneously.

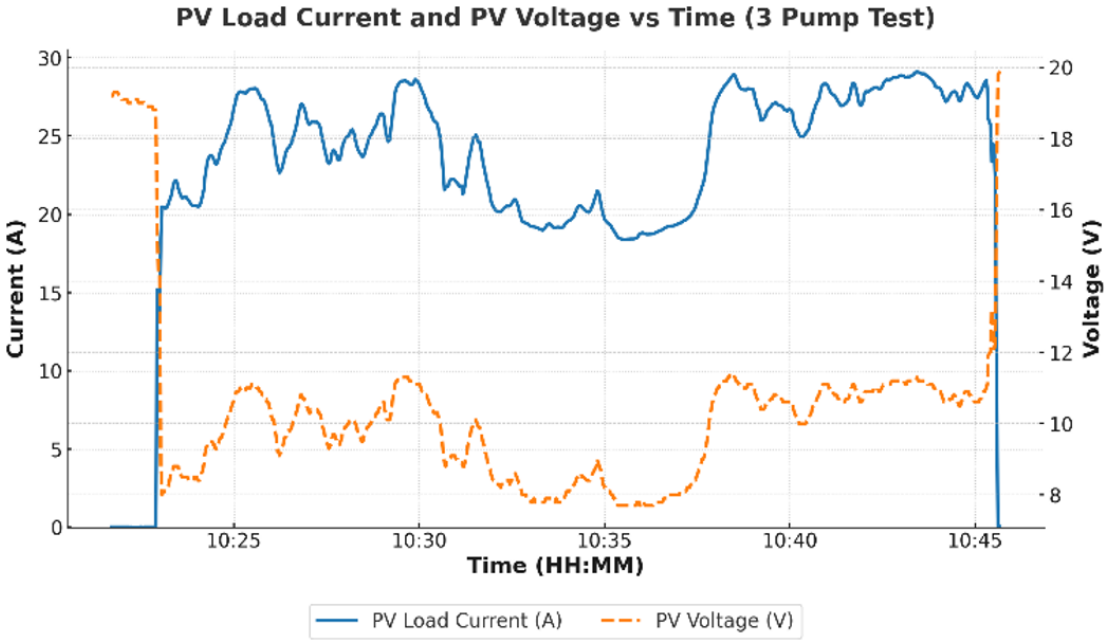

Figure 8. PV voltage and load current versus time for three-pump adaptive operation

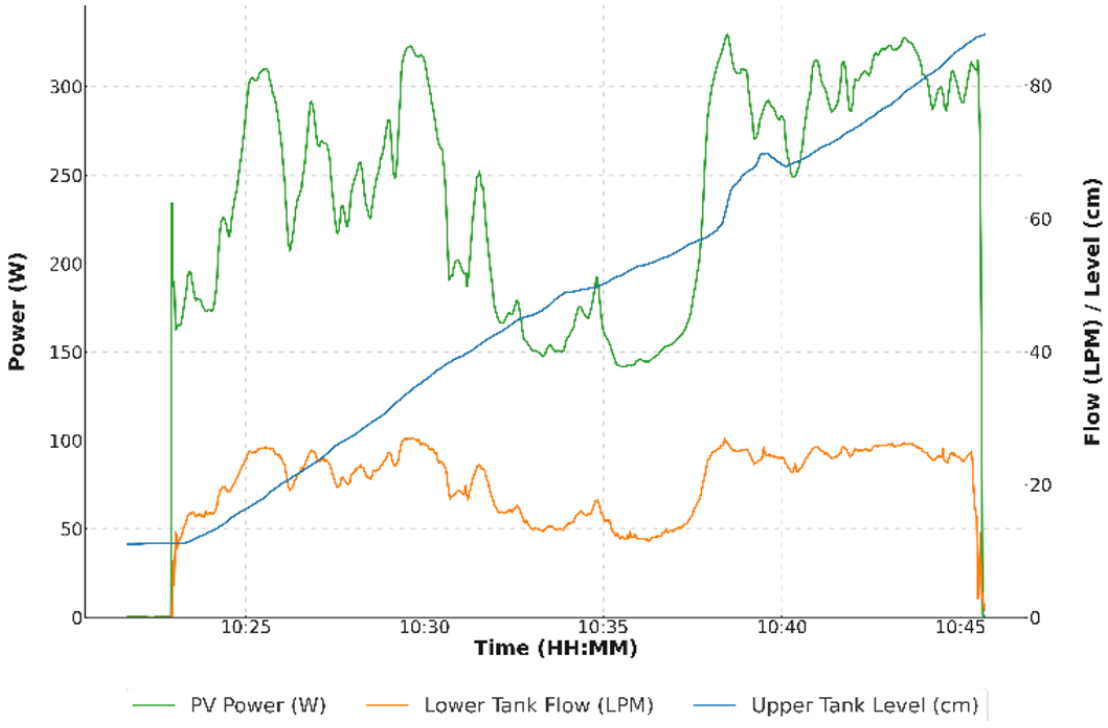

Figure 9. PV power, flow rate, and water level during three-pump operation

In Figure 9, the variation of PV power, flow rate, and upper reservoir water level during the 3-pump test is illustrated. The horizontal axis represents the actual operation time in hours and minutes (HH:MM). The left vertical axis corresponds to PV power (W), while the right vertical axis corresponds to both flow rate (LPM) and upper reservoir level (cm). The three pumps produced the highest PV power and flow rates, resulting in the fastest increase in the upper reservoir level. The initial surge in flow rate was due to the initial response of the pumps and water flow before reaching a more stable operating condition. During the three-pump active phase from 10:22:56 to 10:45:35 (a total duration of 22 minutes and 39 seconds), the PV power (P–PLTS) ranged from 141.60 to 329.30 W with an average of 241.16 W. The flow rate from the lower reservoir (Q–Bottom Tank) varied between 0.00 and 26.91 LPM, averaging 20.41 LPM, while the upper reservoir water level (H–Top Tank) increased from 10.60 cm at the beginning to 85.88 cm at the end of the test (a total rise of 75.28 cm). These results indicate that under the three-pump configuration, the higher PV power and increased discharge flow effectively contributed to a substantial rise in the upper reservoir water level throughout the test period.

4.3 Performance Analysis of Turbine-Generator Configurations

Prior to the turbine–generator efficiency tests, the measurement devices used in the efficiency calculation were verified against calibrated reference instruments using the sensor validation procedure described in the "Testing the Sensors" section. Electrical parameters for power calculation (voltage and current) were measured using PZEM-017 sensors and compared with a FLUKE multimeter, while reservoir water levels were measured using A02YYUW ultrasonic sensors and checked against a ruler; the measured deviations were within acceptable tolerances (Table 1 to Table 4). Flow-rate readings from the inline flow sensors were further checked for consistency with the corresponding reservoir level changes over time. Although a comprehensive uncertainty analysis is beyond the scope of this laboratory-scale study, these verification steps support the reliability of the reported efficiency and energy metrics.

Based on test results, the parallel configuration demonstrated more optimal energy conversion performance than the series configuration. In the parallel configuration, the initial potential energy stored in the upper reservoir (5.09 Wh) at a height of 88.8 cm was successfully converted into 4.878 Wh of electrical energy with an efficiency of 95.83%, as the upper reservoir level decreased to 12.65 cm and the lower reservoir level increased to 85.1 cm within a discharge duration of 34 minutes and 36 seconds, with an average flow rate of 22.95 LPM. Conversely, in the series configuration, the initial potential energy stored in the upper reservoir (5.08 Wh) at a height of 88.7 cm only produced 3.25 Wh of electrical energy due to the pressure drop after passing through the first turbine. With a stable average flow rate of 15.27 LPM, the turbine-generator in the series configuration generated 3.25 Wh of energy throughout the test period. This means that 63.98% of the water's potential energy was successfully converted into electrical energy, and this output value is noticeably lower than the energy output in the parallel configuration.

These results are in line with reported in study [14], that parallel turbine configurations outperform series arrangements at higher flow rates. Moreover, previous research using simulation-based approaches [12, 15], however the present study provides experimental validation under real operating conditions, demonstrating the feasibility of adaptive multi-pump operation driven by PV power.

5 Conclusion

This research aimed to design and test a PHS system to optimize the utilization of fluctuating solar energy. The applied methodology included designing a multi-pump operation based on photovoltaic power availability, integrating an ESP32–NRF24L01-based real-time monitoring and control module with a Raspberry Pi web interface, and testing the performance of the turbine–generator in series and parallel configurations. Test results showed that multi-pump operation significantly increased flow rate and reservoir level rise, with average currents of 13.8 A for one pump, 19.45 A for two pumps, and 24.31 A for three pumps. The turbine–generator test confirmed that the parallel configuration produced higher electrical energy (4.878 Wh; 95.83% efficiency) than the series configuration (3.25 Wh; 63.98% efficiency). The implication of these results was that a parallel configuration was more suitable for supporting a stable and efficient renewable energy supply.

However, this study was limited by the cumulative accuracy of the sensors used, which may have introduced small deviations in the total energy calculation; nonetheless, these effects were considered negligible as all sensors were calibrated within acceptable tolerance ranges. For further research, it is recommended to develop a system with a larger capacity, integrate adaptive control algorithms based on PV power and water levels, and test under varying weather conditions to more comprehensively evaluate the performance of the PHS.

Funding

This research was funded by the Directorate of Research and Community Service, Directorate General of Research and Development, Ministry of Higher Education, Science, and Technology, under the Fundamental Research Regular Scheme, in accordance with Research Contract Number: 060/C3/DT.05.00/PL/2025, Fiscal Year 2025.

Data Availability

The data used to support the research findings are available from the corresponding author upon request.

Conflicts of Interest

The authors declare no conflicts of interest.

References

[1] P. Das, J. Mathur, R. Bhakar, and A. Kanudia, "Implications of short-term renewable energy resource intermittency in long-term power system planning," *Energy Strategy Rev.*, vol. 22, pp. 1–15, 2018. https://doi.org/10.1016/j.esr.2018.06.005

[2] Ministry of Environment and Forestry (Indonesia), "Enhanced Nationally Determined Contribution (E-NDC) of the Republic of Indonesia," Ministry of Environment and Forestry, Republic of Indonesia, Tech. Rep., 2022. https://unfccc.int/sites/default/files/NDC/2022-09/23.09.2022_Enhanced%20NDC%20Indonesia.pdf

[3] Ministry of Environment and Forestry (Indonesia), "Indonesia long-term strategy for low carbon and climate resilience 2050 (lts-lccr 2050)," Ministry of Environment and Forestry, Republic of Indonesia, Tech. Rep., 2021. https://unfccc.int/sites/default/files/resource/Indonesia_LTS-LCCR_2021.pdf

[4] D. F. Silalahi, A. Blakers, M. Stocks, B. Lu, C. Cheng, and L. Hayes, "Indonesia's vast solar energy potential," *Energies*, vol. 14, no. 17, p. 5424, 2021. https://doi.org/10.3390/en14175424

[5] Syafii, A. B. Pulungan, Wati, and R. Fahreza, "Techno-economic analysis of tracker based rooftop PV system installation under tropical climate," *Int. J. Adv. Trends Comput. Sci. Eng.*, vol. 9, no. 4, pp. 6031–6035, 2020. https://doi.org/10.30534/ijatcse/2020/271942020

[6] H. J. C. Conde, C. M. Demition, and J. Honra, "Storage is the new black: A review of energy storage system applications to resolve intermittency in renewable energy systems," *Energies*, vol. 18, no. 2, p. 354, 2025. https://doi.org/10.3390/en18020354

[7] S. Park, N. Yoon, Z. Ullah, B. K. Tarus, B. Choi, H. H. Kim, and M. Son, "Energy storage capability of seawater batteries for intermittent power generation systems: Conceptualization and modeling," *J. Power Sources*, vol. 580, p. 233322, 2023. https://doi.org/10.1016/j.jpowsour.2023.233322

[8] Q. Abbas, H. M. Ali, and A. B. S. Alquaity, "Techno-economic analysis of renewable energy systems with pumped hydro storage for desalinating water in Saudi Arabia," *Int. J. Thermofluids*, vol. 30, p. 101430, 2025. https://doi.org/10.1016/j.ijft.2025.101430

[9] P. C. Nikolaos, F. Marios, and K. Dimitris, "A review of pumped hydro storage systems," *Energies*, vol. 16, no. 11, p. 4516, 2023. https://doi.org/10.3390/en16114516

[10] J. Li, J. Yuan, and X. Yue, "Optimizing multi-objective hybrid energy systems with pumped hydro storage for enhanced stability and efficiency in renewable energy integration," *Eng. Sci. Technol., Int. J.*, vol. 69, p. 102142, 2025. https://doi.org/10.1016/j.jestch.2025.102142

[11] M. Stocks, R. Stocks, B. Lu, C. Cheng, and A. Blakers, "Global atlas of closed-loop pumped hydro energy storage," *Joule*, vol. 5, no. 1, pp. 270–284, 2021. https://doi.org/10.1016/j.joule.2020.11.015

[12] D. Bordeașu, O. Proștean, I. Filip, F. Drăgan, and C. Vașar, "Modelling, simulation and controlling of a multi-pump system with water storage powered by a fluctuating and intermittent power source," *Mathematics*, vol. 10, no. 21, p. 4019, 2022. https://doi.org/10.3390/math10214019

[13] S. Huang, H. Wang, W. Liao, and S. Huang, "Generator side converters coordinated control strategy based on vsc-hvdc dd-pmsg wind turbine series-parallel connection," in *2014 IEEE Conference and Expo Transportation Electrification Asia-Pacific (ITEC Asia-Pacific)*, Beijing, China, 2014, pp. 1–7. https://doi.org/10.1109/ITEC-AP.2014.6940692

[14] M. A. Kriswidijatmoko, R. Hariyanto, and F. A. Widiharsa, "Comparison of the performance of mini generator water turbines in series and parallel flow systems," *TRANSMISI*, vol. 19, no. 2, pp. 114–119, 2023. https://doi.org/10.26905/jtmt.v19i2.12079

[15] N. Yimen, O. Hamandjoda, L. Meva'a, B. Ndzana, and J. Nganhou, "Analyzing of a photovoltaic/wind/biogas/pumped-hydro off-grid hybrid system for rural electrification in sub-Saharan Africa—Case study of Djoundé in Northern Cameroon," *Energies*, vol. 11, no. 10, p. 2644, 2018. https://doi.org/10.3390/en11102644

[16] Z. Serat, "Optimizing renewable energy systems for 100 % clean energy target: A comparative study of solar, hydro, pumped hydro, and battery storage technologies," *J. Energy Storage*, vol. 104, p. 114441, 2024. https://doi.org/10.1016/j.est.2024.114441

[17] M. A. Islam, M. M. N. Ali, T. Mollick, A. Islam, I. B. Benitez, S. S. Habib, A. Al Mansur, M. S. H. Lipu, A. Flah, and M. Kanan, "Assessing the feasibility and quality performance of a renewable energy-based hybrid

microgrid for electrification of remote communities," *Energy Convers. Manag.: X*, vol. 23, p. 100674, 2024. https://doi.org/10.1016/j.ecmx.2024.100674

[18] S. Syafii, F. Azizah, and I. Salfikri, "Solar pumps automation system using programmable logic controller for pumped hydro storage," *Int. J. Power Electron. Drive Syst.*, vol. 15, no. 3, pp. 1517–1525, 2024. https://doi.org/10.11591/ijpeds.v15.i3.pp1517-1525

[19] E. S. Bayu, B. Khan, I. G. Hagos, O. P. Mahela, and J. M. Guerrero, "Feasibility analysis and development of stand-alone hybrid power generation system for remote areas: A case study of Ethiopian rural area," *Wind*, vol. 2, no. 1, pp. 68–86, 2022. https://doi.org/10.3390/wind2010005

[20] H. El Hafdaoui, A. Khallaayoun, and S. Al-Majeed, "Controlled non-dominated sorting genetic algorithms for multi-objective optimal design of standalone and grid-connected renewable energy systems in integrated energy sectors," *IEEE Access*, vol. 13, pp. 14 658–14 685, 2025. https://doi.org/10.1109/ACCESS.2025.3530084

[21] H. Hasabelrasul, Z. Cai, L. Sun, X. Suo, and I. Matraji, "Two-stage converter standalone PV-battery system based on VSG control," *IEEE Access*, vol. 10, pp. 39 825–39 832, 2022. https://doi.org/10.1109/ACCESS.2022.3165664

[22] S. Arya and P. Mahajan, "Introduction to solar cells," in *Solar Cells*. Singapore: Springer Nature, 2023, pp. 1–35. https://doi.org/10.1007/978-981-99-7333-0_1

[23] G. N. Tiwari, A. Tiwari, and Shyam, "Solar cell materials, photovoltaic modules and arrays," in *Handbook of Solar Energy*. Springer, 2016, pp. 123–170. https://doi.org/10.1007/978-981-10-0807-8_4

[24] T. Wu, H. Lin, L. Chen, Z. Liu, Y. Pang, Z. Li, P. Gao, and W. Shen, "Realization of high-voltage output on monolithic silicon solar cells in series for self-powered systems," *Sol. RRL*, vol. 6, no. 7, 2022. https://doi.org/10.1002/solr.202200188

[25] Z. Li, A. Zuo, Z. Mo, M. Lin, C. Wang, J. Zhang, M. H. Hofmann, and A. Jossen, "Demonstrating stability within parallel connection as a basis for building large-scale battery systems," *Cell Rep. Phys. Sci.*, vol. 3, no. 12, p. 101154, 2022. https://doi.org/10.1016/j.xcrp.2022.101154

[26] R. Kamal, M. Abdel-Salam, and M. Nayel, "Output energy and efficiency of a PV module as influenced by stochastic variation of the incident solar irradiation," in *2024 25th International Middle East Power System Conference (MEPCON)*. Cairo, Egypt: IEEE, 2024, pp. 1–7. https://doi.org/10.1109/MEPCON63025.2024.10850215

[27] M. Piliougine, P. Sánchez-Friera, and G. Spagnuolo, "Comparative of IEC 60891 and other procedures for temperature and irradiance corrections to measured I–V characteristics of photovoltaic devices," *Energies*, vol. 17, no. 3, p. 566, 2024. https://doi.org/10.3390/en17030566

[28] N. F. Q. Amran, W. N. A. A. W. Zulkifli, N. Jaalam, F. Arith, and A. S. M. Shah, "Investigation of standard test condition requirement in establishing alternative measurement platform for photovoltaic cell," *J. Phys. Conf. Ser.*, vol. 2928, no. 1, p. 012003, 2024. https://doi.org/10.1088/1742-6596/2928/1/012003

[29] D. Y. Goswami, *Principles of Solar Engineering*. CRC Press, 2015. https://doi.org/10.1201/b18119

[30] A. P. Alonso, "Pumped hydro energy storage systems for a sustainable energy planning," in *Sustainable Energy Planning in Smart Grids*. Elsevier, 2024, pp. 71–89. https://doi.org/10.1016/B978-0-443-14154-6.00014-4

[31] J. K. Schuh, "Utilizing water towers for pumped storage hydropower," in *2023 IEEE Power Energy Conference Illinois (PECI)*. Champaign, IL, USA: IEEE, 2023, pp. 1–7. https://doi.org/10.1109/PECI57361.2023.10197755

[32] Z. Liu, "Development and application of pumped storage power generation system," *E3S Web Conf.*, vol. 606, p. 02003, 2025. https://doi.org/10.1051/e3sconf/202560602003

[33] F. Licheri, M. Petrollese, D. Cocco, and F. Cambuli, "Pumps as turbines for pumped hydro energy storage systems - A small-size case study," *J. Phys. Conf. Ser.*, vol. 2648, no. 1, p. 012046, 2023. https://doi.org/10.1088/1742-6596/2648/1/012046

[34] P. C. Nikolaos, F. Marios, and K. Dimitris, "A review of pumped hydro storage systems," *Energies*, vol. 16, no. 11, p. 4516, 2023. https://doi.org/10.3390/en16114516

[35] R. Sahay and T. N. Swamy, "Micro-hydro power-harnessing the potential energy of water for small-scale electricity generation," *Int. J. Res. Rev. Appl. Sci., Humanit., Technol.*, pp. 13–17, 2024. https://doi.org/10.71143/4p12n447

Nomenclature

G	Solar irradiance intensity	$\mathrm{W/m^2}$
A	Effective surface area of the photovoltaic module	$\mathrm{m^2}$
η	Photovoltaic module efficiency	%
P_{out}	Maximum output power of the photovoltaic module	W
P_{in}	Input solar power incident on the module surface	W
V_{mpp}	Voltage at the maximum power point (MPP)	V
I_{mpp}	Current at the maximum power point (MPP)	A
V_{oc}	Open-circuit voltage	V
I_{sc}	Short-circuit current	A
FF	Fill factor, ratio indicating the squareness of the I–V curve	
m	Mass of water	kg
ρ	Density of water	$\mathrm{kg/m^3}$
V	Volume of water	$\mathrm{m^3}$
g	Gravitational acceleration	$\mathrm{m/s^2}$
H	Elevation difference (head) between upper and lower reservoir	m
E	Gravitational potential energy of water	J or Wh
Q	Water flow rate	$\mathrm{m^3/s}$
t	Flow duration	s